CCFE
CULHAM CENTRE FOR FUSION ENERGY

UK Atomic Energy Authority

UKAEA-CCFE-PR(20)05

N. Zhang, Y. Q. Liu, P. Piovesan, V. Igochine, D. L. Yu, S. Wang, G. Q. Dong, G. Z. Hao, G. L. Xia, W. J. Chen, L. Liu, J. Q. Li, X. Bai

Toroidal modelling of core plasma flow damping by RMP fields in hybrid discharge on ASDEX Upgrade

Toroidal modelling of core plasma flow damping by RMP fields in hybrid discharge on ASDEX Upgrade

N. Zhang, Y. Q. Liu, P. Piovesan, V. Igochine, D. L. Yu, S. Wang, G. Q. Dong, G. Z. Hao, G. L. Xia, W. J. Chen, L. Liu, J. Q. Li, X. Bai

This is a preprint of a paper submitted for publication in Nuclear Fusion

Toroidal modelling of core plasma flow damping by RMP fields in hybrid discharge on ASDEX Upgrade

N. Zhang[1], Y. Q. Liu[2], P. Piovesan[3], V. Igochine[4], D. L. Yu[1], S. Wang[1], G. Q. Dong[1], G. Z. Hao[1], G. L. Xia[5], W. J. Chen[1], L. Liu[1], J. Q. Li[1], X. Bai[1,6], The HL-2A Team, The ASDEX Upgrade Team[7] and The EUROfusion MST1 Team[8]

[1]Southwestern Institute of Physics, P. O. Box 432, Chengdu 610041, China
[2]General Atomics, PO Box 85608, San Diego, CA 92186-5608, USA
[3]Consorzio RFX, Corso Stati Uniti 4, I-35127 Padova, Italy
[4]Max-Planck-Institut für Plasmaphysik, EURATOM Association, Garching, Germany
[5]CCFE, Culham Science Centre, Abingdon OX14 3DB, United Kingdom
[6]Department of Engineering Physics, Tsinghua University, Beijing 100084, Peoples Republic of China
[7]See the author list of H. Meyer *et al.* 2019 Nucl. Fusion 59, 112014
[8]See the author list of B. Labit *et al.* 2019 Nucl. Fusion 59 086020

E-mail: zhangn@swip.ac.cn, liuy@fusion.gat.com

Abstract. Resistive plasma response to the $n = 1$ (n is the toroidal mode number) RMP field is systematically investigated for a high-beta hybrid discharge on ASDEX Upgrade. Both linear and quasi-linear response are modelled using the MARS-F and MARS-Q codes, respectively. Linear response computations show a large internal kink response when the plasma central safety factor q_0 is just above 1. This internal kink response induces neoclassical toroidal viscous (NTV) torque in the plasma core, which is significantly enhanced by the precessional drift resonance of thermal particles in the super-banana regime. Quasi-linear simulation results reveal a core plasma flow damping by about 25%, agreeing well with experimental observations, with the NTV torque playing the dominant role. Sensitivity studies indicate that the internal kink response and the resulting core flow damping critically depend on the plasma equilibrium pressure, the initial flow speed, the coil phasing and the proximity of q_0 to 1. No appreciable flow damping is found for a low β_N plasma. A relatively slower initial toroidal flow results in a stronger core flow damping, due to the enhanced NTV torque. Weaker flow damping is achieved as q_0 is assumed to be farther away from 1. Finally, a systematic coil phasing scan finds the strongest (weakest) flow damping occurring at the coil phasing of approximately 20 (200) degrees, again quantitatively agreeing with experiments. This study points to the important role played by the internal kink response in plasma core flow damping in high-beta hybrid scenario plasmas such as that foreseen for ITER.

Keywords: RMP fields, internal kink response, core flow damping, NTV torque

1. Introduction

It is well known that the high-beta hybrid operation is a promising candidate for offering better energy confinement and obtaining higher fusion gain [1–3]. High-beta hybrid plasma scenarios normally require the plasma pressure to be close to the ideal MHD limit, and the minimal safety factor just above 1 to avoid sawtooth oscillations. Controlling large edge localized modes (ELMs) is a crucial aspect of hybrid operations, including that foreseen for ITER.

Resonant magnetic perturbation (RMP) has been extensively applied to mitigate or suppress ELMs [4–9]. On the other hand, it has been established that RMP fields can easily trigger marginally stable magneto-hydrodynamic (MHD) modes in high pressure plasmas, resulting in a strong resonant field amplification (RFA) effect [10–13]. This RFA effect can potentially deteriorate the performance of hybrid operation, as has been shown in recent ASDEX Upgrade and DIII-D experiments [14]. In experiments, the plasma response to the $n = 1$ RMP field is measured in terms of magnetic perturbations outside the plasma, as well as internal data such as the radial profile of the plasma displacement.

The main finding from the ASDEX Upgrade experiment [14] is that the $n = 1$ hybrid plasma response is the largest in the plasma core region, where the $m = 1$ harmonic component is dominant among the poloidal Fourier spectrum. This is due to the fact that the minimal value of the safety factor, q_{min}, is just above 1. As a consequence, the core plasma toroidal rotation, measured by charge recombination exchange spectrum, was significantly reduced by the RMP field induced $m/n = 1/1$ plasma response. The core plasma flow damping is generally not beneficial to the stability and confinement of tokamak devices, especially in ITER where the plasma core flow is expected to be slow even in the absence of RMP fields.

Plasma flow damping, induced by non-axisymmetric magnetic fields, has been observed on many devices [15–21]. Results indicate that the neoclassical toroidal viscous (NTV) torque plays a potentially important role, though discrepancy still exists between the NTV prediction and experimental observation, especially in the core region [17, 21]. In addition, electromagnetic torque associated with continuum wave resonances can lead to relatively local braking of the plasma flow [22, 23].

In this study, we carry out both linear and quasi-linear plasma response modelling, assuming the $n = 1$ RMP field as in ASDEX Upgrade experiments. The computational tools that we utilize are the MARS-F [24] and MARS-Q [25] codes. For the linear plasma response, several aspects are primarily investigated: (i) comparison of the poloidal spectra between the vacuum field and the plasma response fields [26, 27], (ii) the plasma boundary corrugation due to 3D fields [28], (iii) comparison of toroidal torques evaluated based on linear response fields, including the NTV torque [29] and torques associated with the Maxwell and Reynolds stresses [30]. For the quasi-linear plasma response, we

investigate the (physically) non-linear interaction between the core plasma toroidal flow and the plasma response to the RMP field [31]. The toroidal torques usually act as the sink term in the momentum balance equation, leading to flow damping.

The next section briefly describes the plasma response models. Section 3 describes the ASDEX Upgrade plasma equilibrium and the RMP coil configuration considered in this work. Section 4 reports the main modelling results with the experimental plasma conditions. The dependence of plasma response on the equilibrium pressure, the initial plasma flow, the coil phasing and the on-axis safety factor value, is systematically investigated in Sec. 5. Conclusions are drawn in Sec. 6.

2. Plasma response models

In this work, the plasma response is described by a single fluid resistive MHD model, which includes the equilibrium plasma toroidal flow in full toroidal geometry. The perturbed MHD equations are written for the plasma displacement ξ, the perturbed fluid velocity $\mathbf{v}$, magnetic field $\mathbf{b}$, plasma current $\mathbf{j}$, and pressure p

$$i(\mathbf{\Omega}_{RMP}+n\mathbf{\Omega})\xi = \mathbf{v} + (\xi\cdot\nabla\mathbf{\Omega})R^2\nabla\phi \tag{1}$$

$$\begin{aligned} i\rho(\mathbf{\Omega}_{RMP}+n\mathbf{\Omega})\mathbf{v} = &-\nabla p + \mathbf{j}\times\mathbf{B} + \mathbf{J}\times\mathbf{b} \\ &-\rho[2\mathbf{\Omega}\nabla\mathbf{Z}\times\mathbf{v} + (\mathbf{v}\cdot\nabla\mathbf{\Omega})R^2\nabla\phi] \\ &-\rho\kappa_{\|}|k_{\|}v_{th,i}|[\mathbf{v}+(\xi\cdot\bigtriangledown)\mathbf{V}_0]_{\|} \end{aligned} \tag{2}$$

$$i(\mathbf{\Omega}_{RMP}+n\mathbf{\Omega})\mathbf{b} = \nabla\times(\mathbf{v}\times\mathbf{B}) + (\mathbf{b}\cdot\nabla\mathbf{\Omega})R^2\nabla\phi - \nabla\times(\eta\mathbf{j}) \tag{3}$$

$$i(\mathbf{\Omega}_{RMP}+n\mathbf{\Omega})p = -\mathbf{v}\cdot\nabla P - \Gamma P\nabla\cdot\mathbf{v} \tag{4}$$

$$\mathbf{j} = \nabla\times\mathbf{b} \tag{5}$$

where the variables ρ, $\mathbf{B}$, $\mathbf{J}$ and P denote the equilibrium plasma density, magnetic field, plasma current and pressure, respectively. η is the plasma resistivity. $\mathbf{V}_0 = R\Omega\nabla\phi$ is the toroidal equilibrium flow assumed to be subsonic, where R is the plasma major radius, Ω the toroidal rotation frequency, and ϕ the geometrical toroidal angle. $\Gamma = 5/3$ is the ratio of specific heats. A strong parallel sound wave damping ($\kappa_{\|} = 1.5$) is assumed in the momentum equation (2), mimicking the ion Landau damping [32]. The parallel wave number $k_{\|}$ equals to $(n - m/q)/R$, with m being the poloidal harmonic number and q the safety factor. $v_{th,i} = \sqrt{2T_i/M_i}$ is the thermal ion velocity, where T_i and M_i are the temperature and mass of the thermal ion. We point out that the parallel component is always taken along the equilibrium magnetic field line.

The RMP field is produced by the RMP coil current $\mathbf{j}_{RMP}$ that satisfies

$$\nabla\times\mathbf{b} = \mathbf{j}_{RMP}. \tag{6}$$

Note that the coil current is assumed to be a surface current in our model, with the $\exp(-in\phi)$ dependence along the toroidal angle ϕ. For an AC RMP, Ω_{RMP} denotes the rotating frequency of the applied field. In the ASDEX Upgrade discharge that we will model, one of the rows of the RMP coils provides a rotating field at 10 Hz. This is a slow variation compared to the conducting wall response time (a few milliseconds)

in ASDEX Upgrade. However, the passive stabilizing plates, on which the RMP coils are mounted, have response time in the order of ∼100 milliseconds. The induced eddy currents in these passive plates will therefore reduce the field produced by the rotating row of RMP coils. This complication is not modeled in this work. Instead, we set $\Omega_{RMP} = 0$ in the MARS-Q modeling reported below, meanwhile assuming a given coil phasing that is constant in time.

For the plasma response modelling, the above MHD equations and the coil equation, together with the vacuum equation outside the plasma and the thin wall equation, are numerically solved by the MARS-F code [24] in the toroidal flux coordinate system (s, χ, ϕ), where $s \equiv \psi_p^{1/2}$ represents the radial coordinate, with ψ_p being the normalized equilibrium poloidal flux. χ is the (generic) poloidal angle.

The quasi-linear plasma response model is devised to investigate the self-consistent interplay between the RMP field and the plasma flow. The above $n \neq 0$ linear RMP response equations are solved together with the following $n = 0$ toroidal momentum balance equation

$$\frac{\partial L}{\partial t} = D(L) + T_{NTV} + T_{JXB} + T_{REY} + T_{source} \tag{7}$$

where $L = \rho\langle R^2\rangle \mathbf{\Omega}$ is the surface averaged toroidal momentum of the plasma, and the momentum diffusion operator $D(L)$ is written as

$$D(L) = \frac{G}{s}\frac{\partial}{\partial s}\frac{s}{G}\left[\chi_M\langle|\nabla s|^2\rangle\frac{\partial L}{\partial s} + V_{pinch}\langle|\nabla s|\rangle L\right], \tag{8}$$

with $G \equiv F\langle 1/R^2\rangle$ denoting a geometric factor. Here, F is the equilibrium poloidal current flux function; χ_M represents the toroidal momentum diffusion coefficient, V_{pinch} is the velocity pinch term which we shall ignore in our further modelling.

The NTV torque T_{NTV} follows a semi-analytic model, where various collisionality regimes are smoothly connected [33, 34]. The resonant electromagnetic torque T_{JXB} comes from the field perturbation produced by the external RMP coil. The Reynolds stress torque T_{REY} is produced by the inertial term $\rho(\mathbf{v}\cdot)\mathbf{v}$. Detailed expressions for these torques can be found in our previous work [35]. We mention that these three toroidal torques generally act as sink terms in momentum balance equation. T_{source} is the momentum source term.

In the present work, we assume that the toroidal momentum balance, $D(L(t = 0)) + T_{source} = 0$, has already been reached before the application of the RMP field. Furthermore, we assume that the RMP field does not modify the momentum source term. We only solve for the change of the toroidal momentum $\triangle L = L(t) - L(0)$ relative to the initial value $L(0)$

$$\frac{\partial(\triangle L)}{\partial t} = D(\triangle L) + T_{NTV} + T_{JXB} + T_{REY}, \tag{9}$$

thus bypassing specification of the momentum source term, which enters into our model effectively via the initial flow velocity.

The quasi-linear code MARS-Q [25] is used to solve the above equations as an initial value problem. For the above $n = 0$ momentum equation (9), we assume free boundary

condition at the plasma center and Dirichlet boundary condition at the plasma edge. A semi-implicit, adaptive time stepping scheme is designed for solving the quasi-linear equations. The MARS-Q formulation has been well validated against experiments [36].

3. Plasma equilibrium and coil configuration

The experimental data used in this modelling are extracted from discharge #31034 on ASDEX Upgrade, which is a high-beta hybrid scenario. The normalized beta, $\beta_N \equiv \beta(\%)a(m)B_0(T)/I_p(MA)$, reaches 2.97 at 2400 ms in this discharge. Here, $\beta = \langle P \rangle/(B_0^2/\mu_0)$ is the ratio of the volume averaged plasma pressure to the magnetic pressure, $B_0 = 2.54$ Tesla is the on-axis vacuum toroidal magnetic field and $I_p = 1.04$ MA is the total plasma current. The plasma equilibrium is reconstructed at 2400 ms, using the CLISTE code [37]. The fixed boundary equilibrium code CHEASE [38] is then utilized to refine the CLISTE output and to produce input for MARS-F/Q. The radial profiles of the key equilibrium parameters, including the plasma density, the plasma pressure, the safety factor and the toroidal rotation, are shown in Fig. 1. Note that the

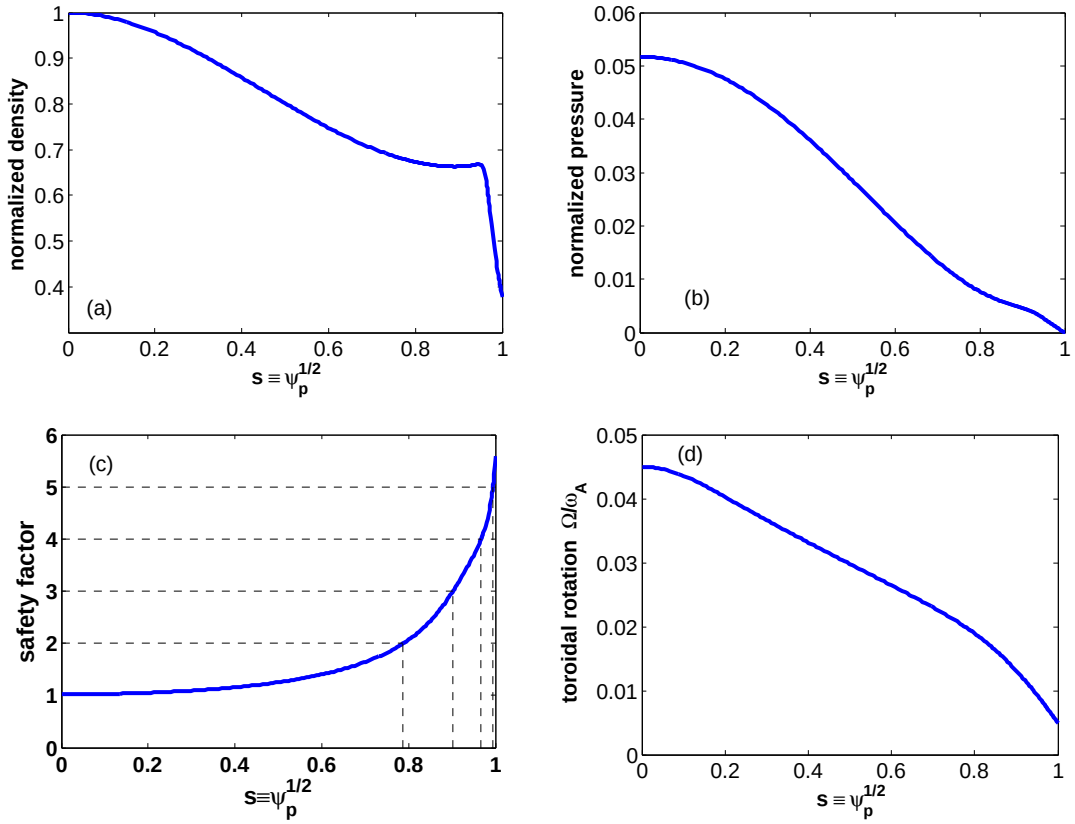

Figure 1: The radial profiles of equilibrium quantities: (a) the plasma density normalized to unity, (b) the plasma pressure normalized by B_0^2/μ_0, (c) the safety factor q (the on-axis safety factor $q_0 = 1.02$), (d) the plasma toroidal rotation normalized by the ω_A. ψ_p is the normalized equilibrium poloidal flux.

plasma pressure shown here is normalized by B_0^2/μ_0. The plasma density is normalized to unity at the magnetic axis. The on-axis safety factor q_0 is just above 1, based on the measurement of the motional Stark effect (MSE). The profile of the toroidal rotation, shown in Fig. 1(d), was measured by the charge exchange recombination spectroscopy (CXRS) system.

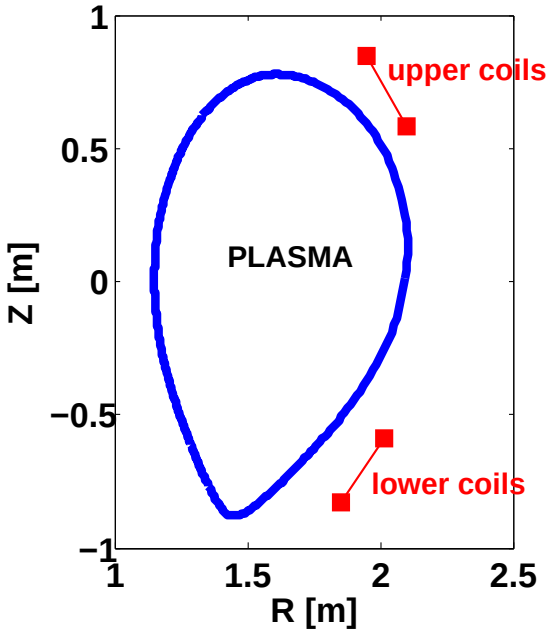

Figure 2: The location of the RMP coils and plasma boundary shape on the (R, Z)-plane for the discharge 31034 at 2400ms.

Figure 2 plots the plasma boundary shape, together with the location of the RMP coils on the (R, Z)-plane. The RMP coils (the B-coils) on ASDEX Upgrade include two rows, each consisting of eight equally distributed coils along the toroidal angle [39]. Each coil has 5 turns, with the total coil current of 5 kAt in this experiment (as well as in our further modelling). In both the experiment and modelling, the coils are arranged to produce predominantly the $n = 1$ vacuum field.

4. Modelling results

Both linear and quasi-linear plasma responses to the $n = 1$ vacuum RMP fields are studied. Even parity coil phasing (between the upper and lower rows) $\Delta\phi^{U/L} = 0$ is assumed in this section. [Results with coil phasing scan will be reported in section 5.] The plasma resistivity is assumed to be uniform along the minor radius, with the magnetic Lundquist number $S \equiv \tau_R/\tau_A = 10^7$, where $\tau_R = \mu_0 a^2/\eta$ is the resistive diffusion time and $\tau_A = R_0\sqrt{\mu_0\rho_0}/B_0 = 1/\omega_A$ is the on-axis Alvén time. We also varied the resistivity amplitude (by two orders of magnitude) as well as its radial profile (uniform model versus Spitzer model), and found that both the computed plasma

displacement and the eventual core flow damping is not sensitive to the plasma resistivity model that we assume here. In what follows, we start by reporting the linear plasma response results computed by MARS-F.

4.1. Linear response results

Figure 3(a-b) compares poloidal spectra of the $n = 1$ radial magnetic field, between the vacuum field and that including the plasma response. The perturbed radial field is defined as

$$b^1 = \frac{q}{R_0^2} \frac{\mathbf{b} \cdot \nabla \psi}{\mathbf{B}_{eq} \cdot \nabla \phi} \tag{10}$$

where $\mathbf{B}_{eq}$ is the equilibrium magnetic field. Note that the Fourier harmonics of b^1 are

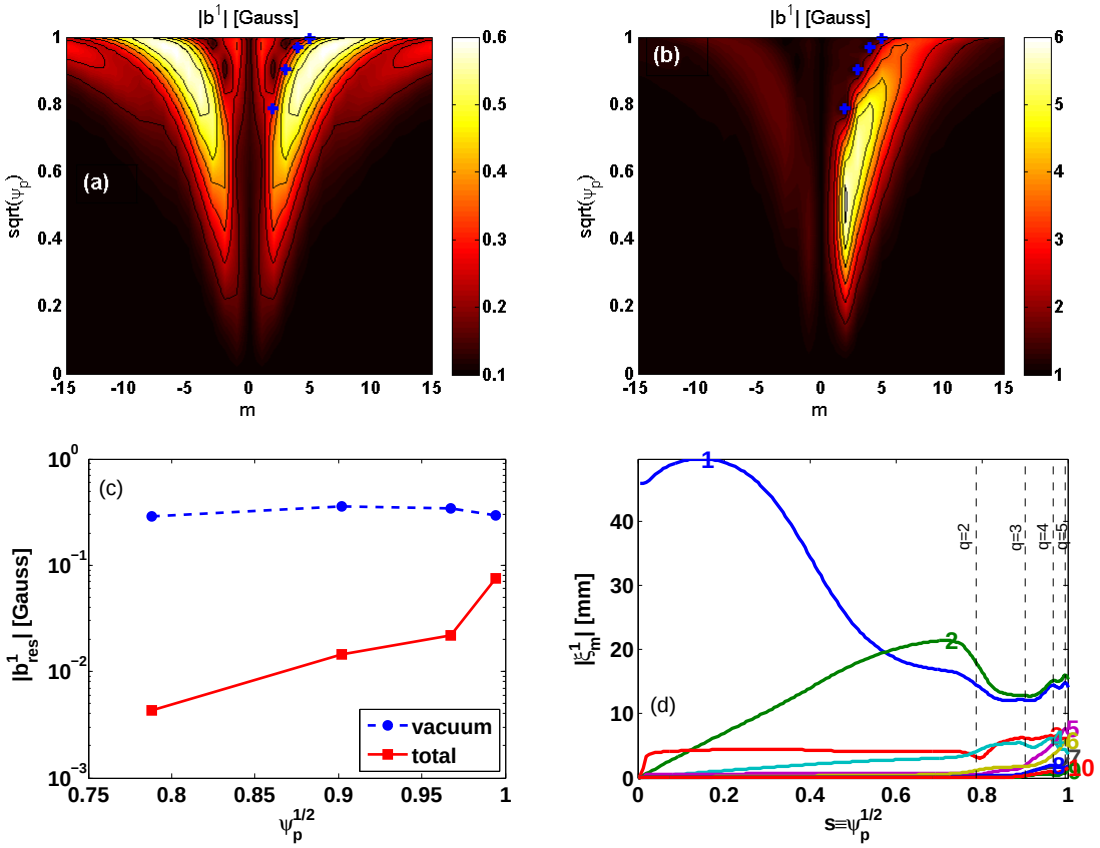

Figure 3: The computed poloidal spectra of (a) the vacuum fields, (b) the plasma response fields. The poloidal Fourier harmonic is decomposed in a straight-file-line (SFL) flux coordinate system. The symbol + labels the location of $q = m/n$ rational surfaces. Comparison of (c) the resonant harmonic amplitude for the perturbed radial field b^1_{res} between the vacuum and response fields. The Fourier harmonics of (d) the computed radial displacement of the plasma. Vertical dashed lines indicate the radial location of the rational surface. The normalized beta β_N is 2.97. The RMP coil current is assured to be even parity ($\Delta\phi^{U/L} = 0$).

defined in a straight-field-line flux coordinate system in these plots.

The key observation from Fig. 3 is the strong amplification (factor of ~ 10) of the vacuum field by the plasma response, for this ASDEX Upgrade plasma. This strong amplification, driven by high plasma pressure, has significant consequence on the plasma core flow damping as will be shown later on. The amplification occurs in the positive ($m > 0$) half of poloidal spectrum, which covers the resonant harmonics. The effect of the plasma response on the vacuum field is minor for the negative ($m < 0$) half of (non-resonant) harmonics.

For this plasma configuration, even parity B-coil currents do not produce large vacuum resonant field components. Nevertheless, plasma response further reduces the resonant components as shown by Fig. 3(c). The reduction is in fact substantial, by $1 \sim 2$ orders of magnitude.

Figure 3(d) plots the the radial distribution of the poloidal Fourier harmonics for the computed plasma radial displacement ($\xi^1 = \xi \cdot \nabla s$). It is evident that a large $m/n = 1/1$ internal kink component is excited by the applied RMP field. This is mainly due to the fact that the on-axis safety factor q_0 is close to 1, and the central magnetic shear is relatively weak (cf. Fig. 1(c)).

The large internal kink response, reported above, has direct consequence on the plasma core flow damping, as will be demonstrated in the next subsection. Before reporting quasi-linear simulation results, however, we examine the toroidal torques associated with the linear plasma response fields.

Figure 4 compares radial distribution of three toroidal torques, computed using the afore-reported linear response fields. The NTV torque is the largest among three torques in the plasma core region. Note that the NTV torque is proportional to square of the perturbed magnetic field in the Lagrangian form. The Lagrangian field in turn is largely proportional to the plasma displacement. The large internal kink component in the plasma response, shown in Fig. 3(d), is thus responsible for the large core NTV torque.

The NTV torque density is relatively small in the middle of the plasma column ($s \equiv \psi_p^{1/2} \sim 0.3 - 0.9$). The electromagnetic torque generally dominates in this region. The NTV torque, however, becomes dominant again in a narrow region near the plasma edge ($s \sim 0.95$). In order to understand this behavior, we examine the NTV physics in more detail in Fig. 5.

The NTV torque is generally sensitive to wave-particle resonance conditions in the (thermal) particle velocity space. Consequently, the NTV torque can come from both resonant and non-resonant contributions. The former occurs when the toroidal precessional drift frequency of trapped thermal particles (mostly thermal ions) is larger than or comparable to the plasma $\mathbf{E} \times \mathbf{B}$ rotation frequency. Figure 5(a) plots both the resonant and non-resonant contributions, together with the total NTV torque. In the core and a narrow region near the plasma edge, the NTV torque is predominantly contributed by the resonant portion. Only in the middle of the plasma column, the non-resonant contribution dominates.

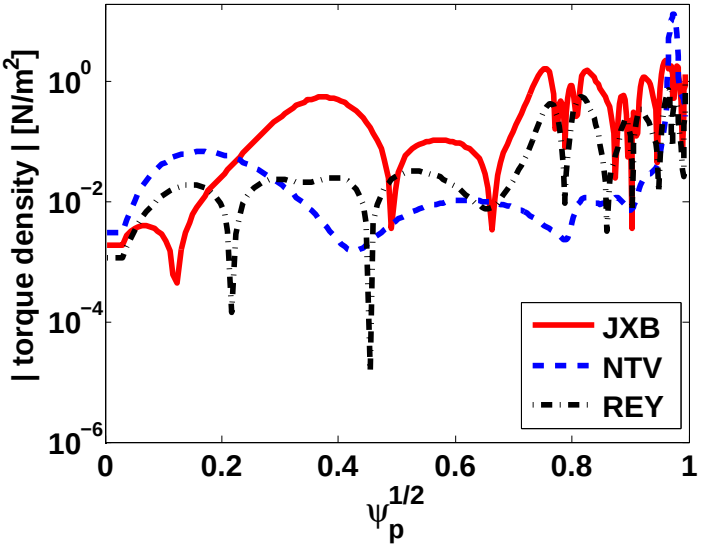

Figure 4: Comparison of various toroidal torque densities - the resonant electromagnetic torque (JXB), the neoclassical viscous torque (NTV), and the torque due to the Reynolds stress (REY). The RMP coil current is assured to be even parity ($\Delta\phi^{U/L} = 0$).

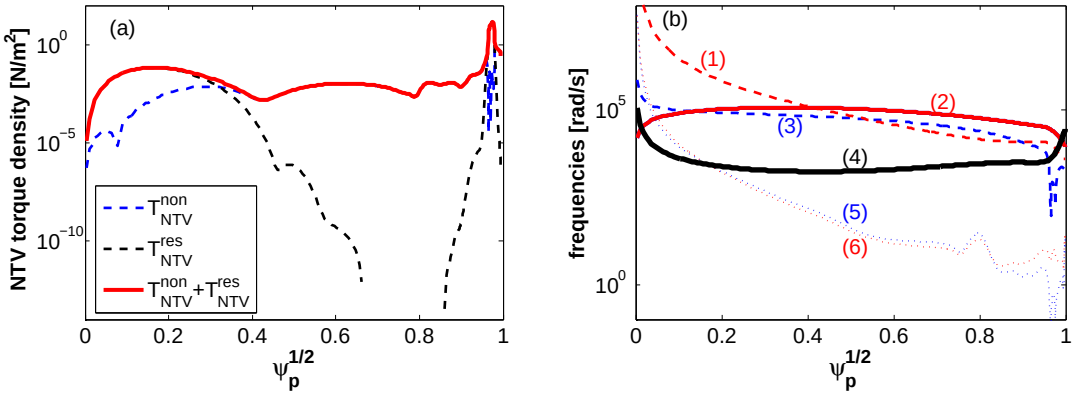

Figure 5: (a) The NTV torque density profiles including both non-resonant (T^{non}_{NTV}) and resonant (T^{res}_{NTV}) contributions. (b) Radial profiles of various frequencies and boundaries separating collisionality regimes for the NTV torque: curve (1) is ω_D/ϵ, with ω_D being the precession drift frequency of trapped thermal ions and ϵ being the inverse aspect ratio; curve (2) represents $\epsilon^{1/2}\omega_{ti}$, with ω_{ti} being the thermal ions transit frequency; curve (3) is the $\mathbf{E}\times\mathbf{B}$ rotation frequency ω_E; curve (4) is the ion-ion effective collision frequency ν/ϵ; curve (5) represents $\omega_E(\delta B/\epsilon)^2$, where δB is the amplitude of the surface averaged perturbed magnetic field; curve (6) is $\omega_D(\delta B/\epsilon)^{3/2}$.

Figure 5(b) plots various frequencies and boundaries separating collisionality regimes for the NTV torque. In both the core region and a small region near the plasma edge, the $\mathbf{E}\times\mathbf{B}$ frequency (curve (3)), which represents the RMP field frequency in the plasma frame, does not exceed the precessional drift frequency (curve (1)) of trapped thermal ions. The wave-particle resonance condition is well satisfied in these two plasma regions, leading to resonant NTV torque contribution. Note that the thermal ion-ion collision frequency (curve (4)) is generally low compared to the other two drift frequencies ((1) and (3)), except near the very edge of the plasma. Too frequent particle collision tends to annihilate the wave-particle resonance. The core resonant NTV enters into the so-called super-banana regime when curve (4) is below (6). With curve (4) being between (3) and (6), as well as curve (3) being below curve (1), the NTV torque is in the super-banana plateau regime. For this ASDEX Upgrade plasma, the core NTV torque thus covers both super-banana and super-banana plateau regimes. In the middle of the plasma column ($s\sim 0.5-0.9$), the non-resonant NTV torque is in the $\sqrt{\nu}$-regime, when the thermal ion collision frequency is between curve (3) and (5).

We note that the precessional drift frequency, curve (1), only represents an 'average' value - the 'local' frequency, that participates in the wave-particle resonance, depends on the particle pitch angle as well as the particle energy. We also note that the thermal electron collision frequency is typically much higher than that of ions. Consequently, the resonant NTV contribution from trapped thermal electrons is normally much smaller than that from thermal ions. Only the thermal ion NTV torque is included in the present study.

The radial profile of the electromagnetic (JXB) torque density is rather global in the middle region ($s\sim 0.2-0.8$), contrary to the conventional understanding that the electromagnetic torque should be strongly localized near rational surfaces. This 'widening' effect results from the 'resonant splitting' phenomenon [22] , which occurs when the perturbation field (as a wave) rotates in the plasma frame, and thus is in resonance with plasma continuum waves (sound wave and shear Alfvén wave). The applied dc RMP field corresponds to a rotating wave in the plasma frame. Finally, we mention that the toroidal torque, associated with the Reynolds stress tensor, is generally small and does not provide dominant contribution to the total torque in this ASDEX Upgrade plasma.

4.2. Quasi-linear response results

The MARS-Q quasi-linear simulations assume a numerically adjustable parameter χ_M for the momentum diffusion. In the present study, we choose $\chi_M \sim 1$ m^2/s, which is a value not far from present-day experiments. A detailed study of the effect of momentum diffusion on flow damping, by scanning χ_M, has previously been performed [36].

The quasi-linear simulation results are summarized in Fig. 6. The strongest flow damping occurs in the plasma core region (Fig. 6(a)). Time traces of the toroidal rotation frequency, at the magnetic axis as well as at rational surfaces (Fig 6(b)), show

that the on-axis flow is quickly damped at the initial stage of the simulation. The flow profile reaches a steady state after $\sim 200 - 300$ ms. The 'saturated' rotation frequency is about 25% lower than the initial rotation in the plasma core. This degree of reduction quantitatively agrees with experimental measurements [14].

We point out that, despite the good agreement between modeling and experiments shown above, caution has to be taken by two reasons. First, as mentioned before, we do not include the eddy current effect from the conducting plates, which will somewhat reduce the applied vacuum field reaching the plasma region (for one of the rows of the RMP coils). On the other hand, as will be shown in the next section, the MARS-Q

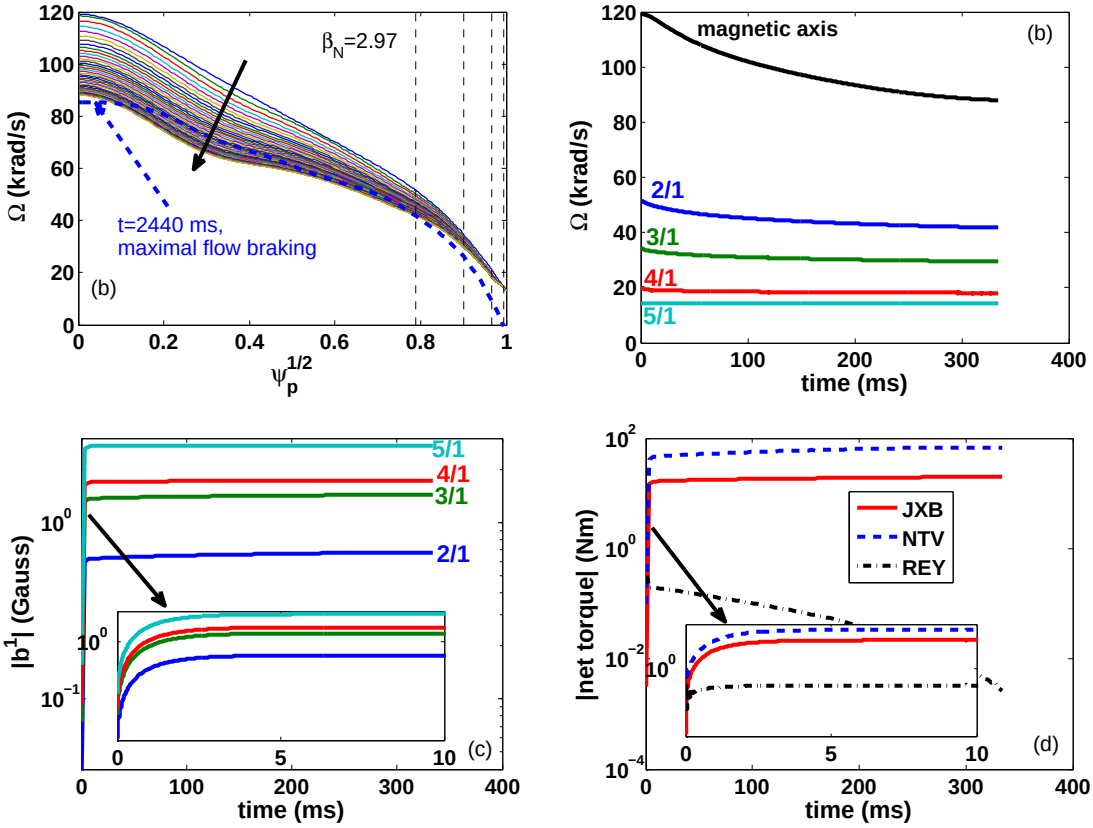

Figure 6: The evolution of (a) the radial profile of plasma flow, computed from quasi-linear response simulation. The arrow indicates the time flow, and only 41 time slices are plotted for the evolution of radial flow profile, and equally spaced in time. The blue dashed curve represents the radial profile of toroidal plasma flow based on the CXRS measurements for this ASDEX Upgrade discharge at 2440 ms (maximal flow braking). The time evolution of (b) the plasma flow amplitude at the magnetic and rational surfaces, (c) the amplitude of the resonant poloidal harmonics (in the straight-field-line coordinate system) of the perturbed radial magnetic field at the corresponding rational surface, and (d) the amplitude of the net torques acting on the overall plasma. The normalized beta β_N is 2.97. The RMP coil current is assured to be even parity ($\Delta\phi^{U/L} = 0$).

results are also sensitive to some of the plasma parameters. For instance, larger than 25% fraction of core flow damping is obtained, if we start the MARS-Q simulation with lower plasma flow.

Figure 6(c) shows that the amplitude of the resonant field components saturates to the level of several Gauss during the flow damping. In addition, the eventual stable solutions also indicates that a *linearly* stable $m = 1$ internal kink mode response is triggered for this case. The evolution of net torques are compared in the Fig. 6(d). The net NTV torque is far greater than the net Maxwell and Reynolds stress torques. This also holds for other cases reported in section 5. Therefore, for this ASDEX Upgrade plasma, we conclude that the NTV torque plays the dominant role in the core plasma rotation damping.

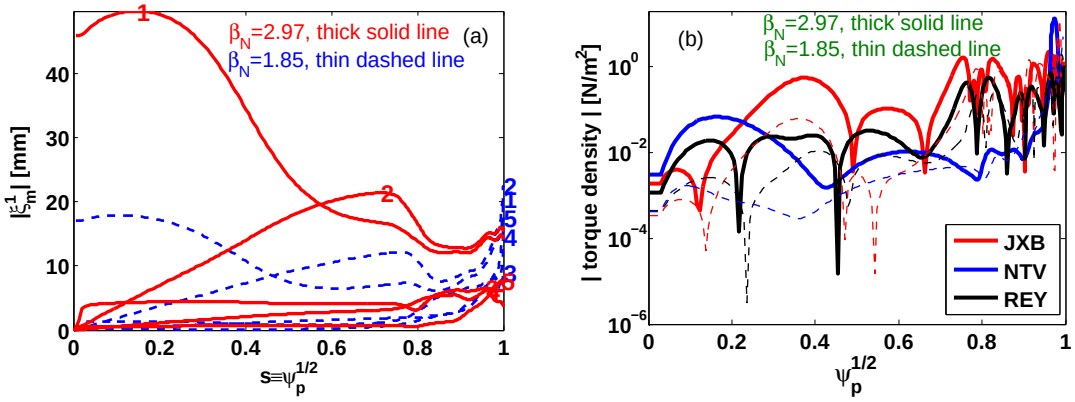

Figure 7: Comparison of (a) the poloidal Fourier harmonics of the computed plasma radial displacement (only the harmonics with $m = 1 \sim 5$ are presented), and (b) the toroidal torque radial distribution for the different plasmas pressure. Shown in thick solid (thin dashed) lines are the results with $\beta_N = 2.97$ ($\beta_N = 1.85$). The RMP coil current is assured to be even parity ($\Delta\phi^{U/L} = 0$).

5. Sensitivity studies versus key simulation parameters

5.1. Effect of plasma pressure

It has been established that the resonant field amplification effect is sensitive to the plasma pressure [12]. This motivates us to investigate the linear and quasi-linear response of a relative low pressure plasma to the applied RMP fields. In this subsection, we artificially reduce the plasma pressure to the level ($\beta_N = 1.85$) that corresponds to an earlier time in the same discharge. Other parameters are the same as that from the reference case reported in section 4.

Figure 7(a) compares radial profiles of the dominant poloidal Fourier harmonics for the MARS-F computed plasma radial displacement, as a result of the linear plasma response. It is evident that, compared to the lower pressure case, the plasma

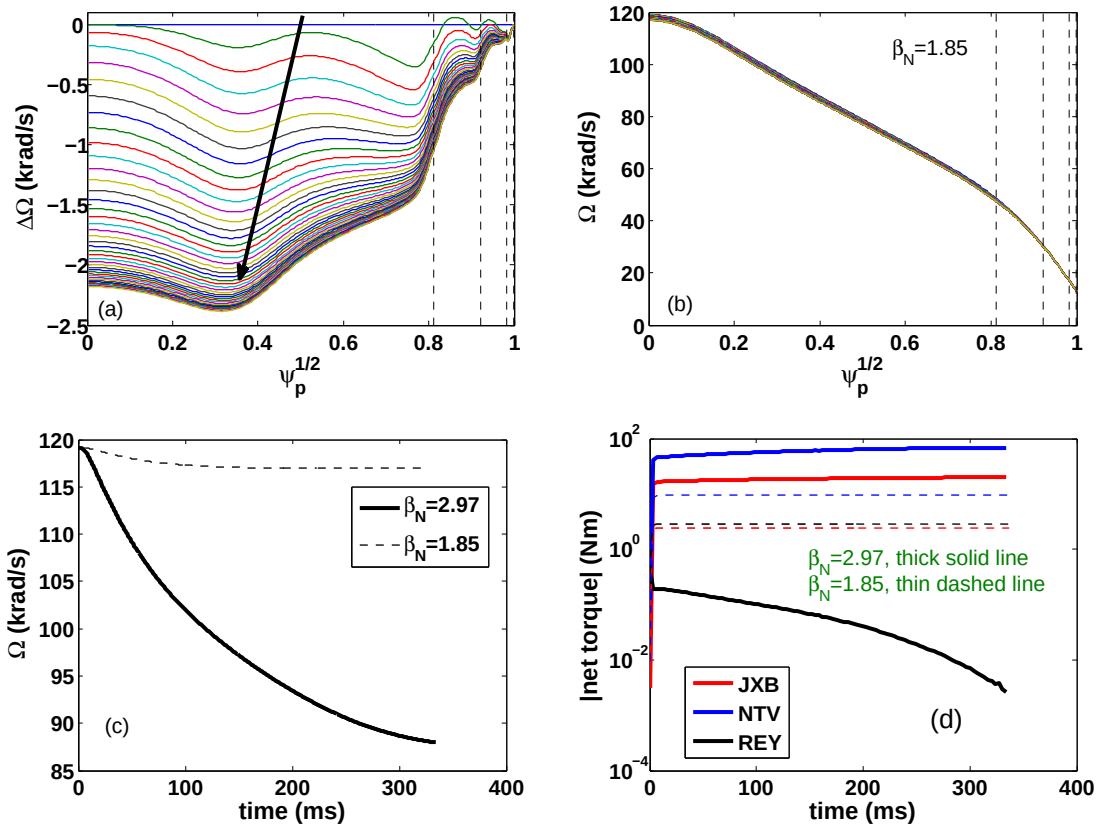

Figure 8: The evolution of (a) the change of plasma flow radial profile, and (b) the total of plasma flow radial profile, computed from quasi-linear response simulation. The arrow in (a) indicates the time flow, and only 41 time slices are plotted for the evolution of radial flow profile, and equally spaced in time. Comparison of the time evolution of the (c) amplitude of the plasma rotation at the magnetic axis, and (d) amplitude of the net torques acting on the overall plasma for the different plasmas pressure. Shown in thick solid (thin dashed) lines are the results with $\beta_N = 2.97$ ($\beta_N = 1.85$). The RMP coil current is assured to be even parity ($\Delta\phi^{U/L} = 0$).

displacement (representing the plasma response here) is substantially enhanced at the experimental pressure value. In particular, the $m/n = 1/1$ component is increased by more than factor of 2. This overall strong amplification (over the applied vacuum field) by high pressure plasma is also evident by the perturbed magnetic field as already shown in Fig. 3. We also note that, for the $\beta_N = 1.85$ case, the amplitude of the external kink component is comparable to that of the internal kink, due to larger edge peeling response which occurs when the edge safety factor is close to an integer number ($q_a = 5.04$ here) [11].

As a result of strong amplification at high plasma pressure, the computed quasi-linear toroidal torques are also much larger than that of the low-pressure case (Fig. 7(b)). In particular, the large $m/n = 1/1$ internal kink response results in much larger core NTV torque at high pressure. It is this large NTV torque that is eventually responsible

for the core flow damping found in MARS-Q simulation as reported in Fig. 6, as well as observed in experiments.

Indeed, the core flow damping is much weaker for the the low-pressure case, as found by MARS-Q quasi-linear simulation reported in Fig. 8. The simulated core flow damping in less than 2% for the low pressure case, as compared to the 25% reduction for the high pressure case. This is also confirmed by comparing time traces of the net toroidal torques, shown in Fig. 8(d). Both the NTV torque (the dominant one) and the electromagnetic torque is much larger for the high pressure plasma. Interestingly, the Reynolds stress torque is smaller in the high pressure case. On the other hand, the Reynolds stress torque is very small in both plasmas, and its role in flow damping can be neglected. Figure 8 thus leads to a conclusion that high plasma pressure for the considered ASDEX Upgrade plasma is the key to observed finite core flow damping, as a result of strong field amplification at high pressure.

5.2. Effect of initial flow amplitude

It is known that the NTV torque is sensitive to plasma initial flow. Slow flow facilitates entrance into the resonant NTV regime, which can significantly enhance the NTV torque. It is thus expected that the degree of flow damping should depends on the amplitude of the initial plasma flow. Figure 9 compares the radial profiles of the MARS-F computed plasma displacement as well as the three toroidal torques, between two cases - with the experimentally measured flow and with the artificially reduced flow.

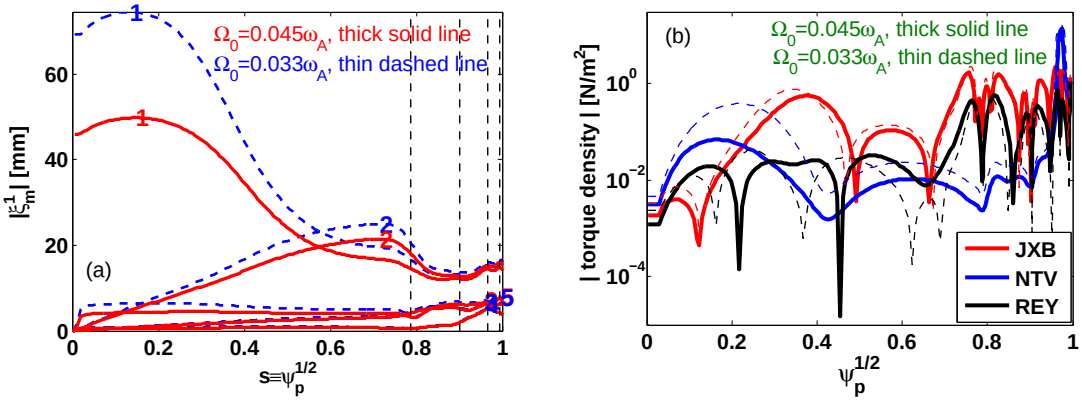

Figure 9: Comparison of (a) the poloidal Fourier harmonics of the computed plasma radial displacement (only the harmonics with $m = 1 \sim 5$ are presented), and (b) the toroidal torque radial distribution. Shown in thick solid (thin dashed) lines are the results with $\Omega_0 = 0.045\omega_A$ ($\Omega_0 = 0.033\omega_A$). The RMP coil current is assured to be even parity ($\Delta\phi^{U/L} = 0$).

In the latter case, the on-axis plasma flow is reduced from $0.045\omega_A$ to $0.033\omega_A$, with the overall profile shape scaled by the same factor. Note that the $m/n = 1/1$ internal kink component is ~50% larger at reduced plasma flow. This is another factor (in addition to

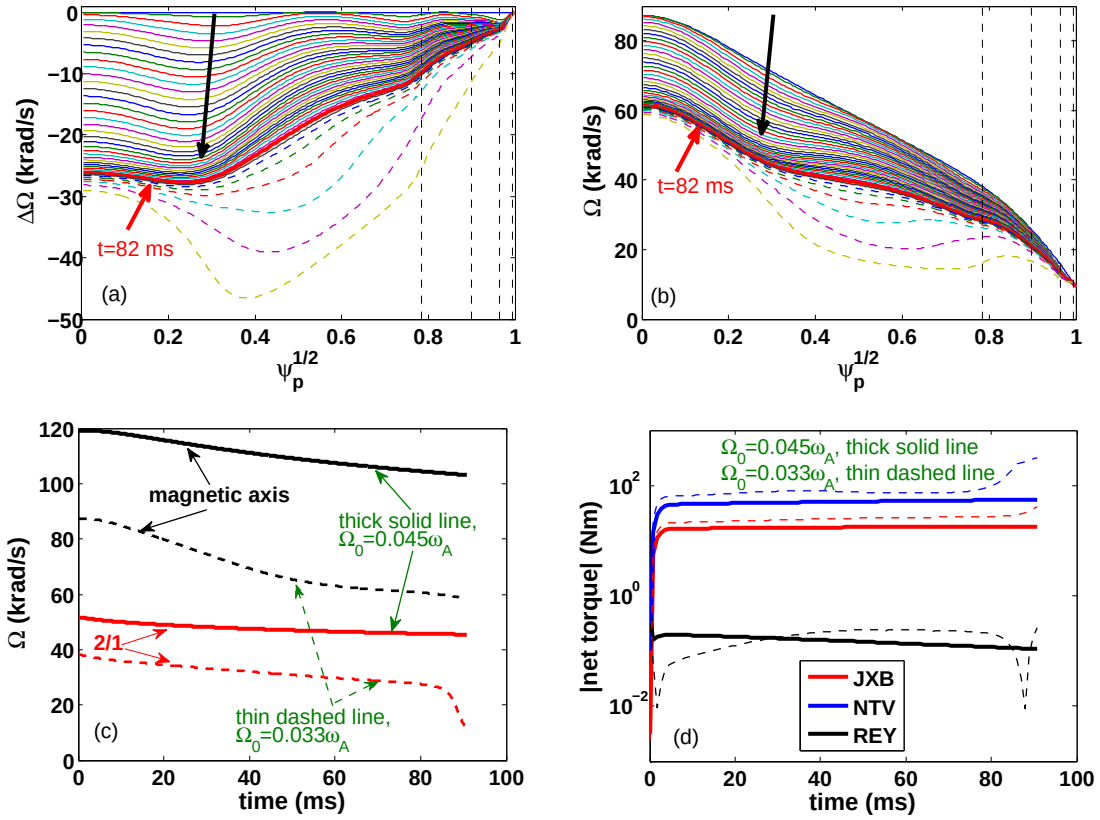

Figure 10: The evolution of (a) the change of plasma flow radial profile, and (b) the total of plasma flow radial profile, computed from quasi-linear response simulation. The arrows in (a) and (b) indicate the time flow, and only 41 time slices are plotted for the evolution of radial flow profile, and equally spaced in time. Comparison of the time evolution of the (c) amplitude of the plasma rotation at the magnetic axis and $q = 2$ rational surface, and (d) amplitude of the net torques acting on the overall plasma for the different plasmas flow. Shown in thick solid (thin dashed) lines are the results with $\Omega_0 = 0.045\omega_A$ ($\Omega_0 = 0.033\omega_A$). The RMP coil current is assured to be even parity ($\Delta\phi^{U/L} = 0$).

the more resonant NTV regime at slower flow) that leads to substantial increase of the core NTV torque as shown in Fig. 9(b). Note also that both the Maxwell and Reynolds stress torques are not much affected by reduction of the plasma flow.

The above results from MARS-F linear response computation are also confirmed by the MARS-Q quasi-linear simulation reported in Fig. 10. Starting from a reduced initial flow, MARS-Q finds a larger core flow damping - exceeding 30% - within the first $t = 82$ ms of simulation time. However, no steady state solution is found after 82 ms. Instead, a rapid flow damping starts to develop in the middle of the plasma column (Fig. 10(a-b)), including that at the $q = 2$ surface (Fig. 10(c)). Further simulation leads to a complete flow damping and numerical crash of the simulation. Numerical crash occurs since quasi-linear model does not capture full non-linear physics (e.g the

large 2/1 island physics), which becomes important near the end of simulation.

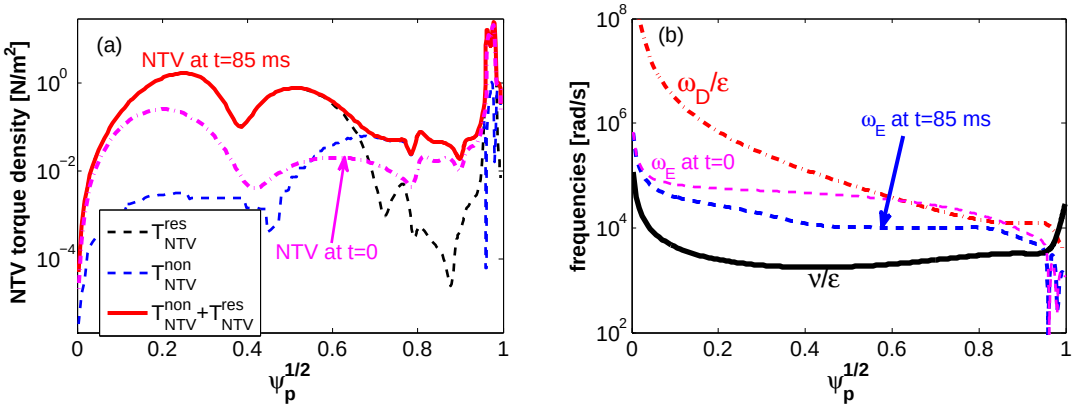

Figure 11: (a) The NTV torque density profiles including both non-resonant (T^{non}_{NTV}) and resonant (T^{res}_{NTV}) contributions. Here the radial profile of plasma flow at the moment of $t = 85$ ms is used to compute the NTV torque. Radial profile of (b) the magnetic precession drift frequency of trapped thermal ions ω_D/ϵ, the $\mathbf{E} \times \mathbf{B}$ rotation frequency ω_E, the ion-ion effective collision frequency ν/ϵ. ϵ is the inverse aspect ratio. Note the pink curves indicate the radial profile of the NTV torque (a) and the $\mathbf{E} \times \mathbf{B}$ rotation frequency (b) amplitude at the initial moment of quasi-linear simulation ($t = 0$).

It turns out that the rapid flow damping in the plasma middle region, at the time after 82 ms, is caused by the substantially enhanced NTV torque in that region as shown by Fig. 11(a), which in turn is due to the reduced $\mathbf{E} \times \mathbf{B}$ drift frequency as shown in Fig. 11(b). As a result, the net NTV torque rapidly grows after 82 ms (Fig. 10(d)), leading to a strong rotation braking in this case. We mention that in experiments, a mode locking eventually occurred, accompanied by further damping of plasma flow [14]. Our quasi-linear simulation with reduced initial flow appears to be consistent with this scenario.

5.3. Effect of coil phasing

The results reported so far are obtained by assuming even parity ($\Delta\phi^{U/L} = 0$) coil phasing for the B-coils in ASDEX Upgrade. The coil phasing $\Delta\phi^{U/L}$ has also been continually varies in experiments. In this subsection, we study the effect of coil phasing on the linear and quasi-linear response.

Amplitude of the normal displacement ($\xi_n = \xi^1 / \mid \nabla s \mid$) of the plasma, at the radial location of $s = 0.2$, is computed according to the linear response model and plotted in Fig. 12(a) as a function of $\Delta\phi^{U/L}$. The maximal (minimal) plasma response occurs when the differential phase $\Delta\phi^{U/L}$ equals to about 20 (200) degree. Radial profiles of the Fourier harmonics for the displacement are compared between the $\Delta\phi^{U/L} = 20^o$ and 200^o coil phasing in Fig. 12(b), showing that the response can be globally maximized (minimized), by choosing the proper coil phasing.

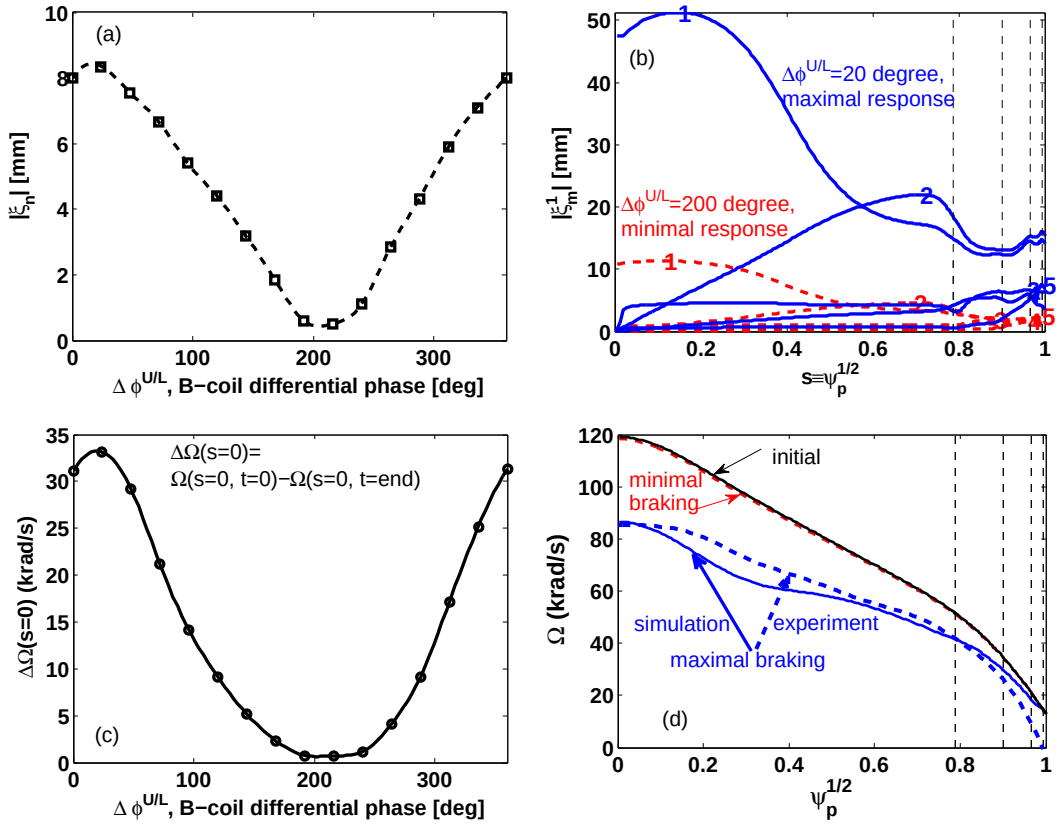

Figure 12: The amplitude of (a) the plasma surface displacement ($\xi_n = \xi^1/\mid \nabla s \mid$) at the location of $s = 0.2$ versus the toroidal phasing $\Delta\phi^{U/L} = 0$ of the coil currents. Comparison of (b) the poloidal Fourier harmonics of the computed plasma radial displacement (only the harmonics with $m = 1 \sim 5$ are presented) for the maximal and minimal response. The amplitude of (c) the change of plasma rotation at the magnetic axis, with $\Omega_0(t = end)$ corresponding to the saturated amplitude. Comparison of (d) the radial profile of the final plasma rotation for the maximal and minimal response. The blue dashed curve represents the radial profile of toroidal flow based on the CXRS measurements for this ASDEX Upgrade discharge at 2440 ms (maximal flow braking).

The MARS-Q quasi-linear computations are carried out for a number of coil phasing values, with results (the amount of on-axis rotation damping $\triangle\Omega(s = 0) = \Omega(s = 0, t = 0) - \Omega(s = 0, t = t_{\rm end})$, $t_{\rm end}$ is the time when solution reaches steady state) summarized in Fig 12(c). It is interesting, albeit not surprising, that the dependence of the flow damping on the coil phasing, obtained from quasi-linear simulations, follows that of plasma displacement from linear computations as shown by Fig. 12(a). The on-axis flow damping shown in Fig 12(c) is also well indicative to the whole rotation profile damping, as shown by Fig. 12(d). In particular, we note that almost no flow damping occurs with the coil phasing of $\Delta\phi^{U/L} = 200^{\rm o}$. These results agree well with the experimental measurements (cf. figure 5 from Ref. [14]).

5.4. Variation of on-axis safety factor q_0

The stability of the internal kink mode is sensitive to the q_0 value, motivating our investigation on the effect of q_0 on the plasma core flow damping. Here, we again start with the reference case reported in section 4, and vary the equilibrium q_0. This is achieved by slightly varying the total plasma current without modifying the current

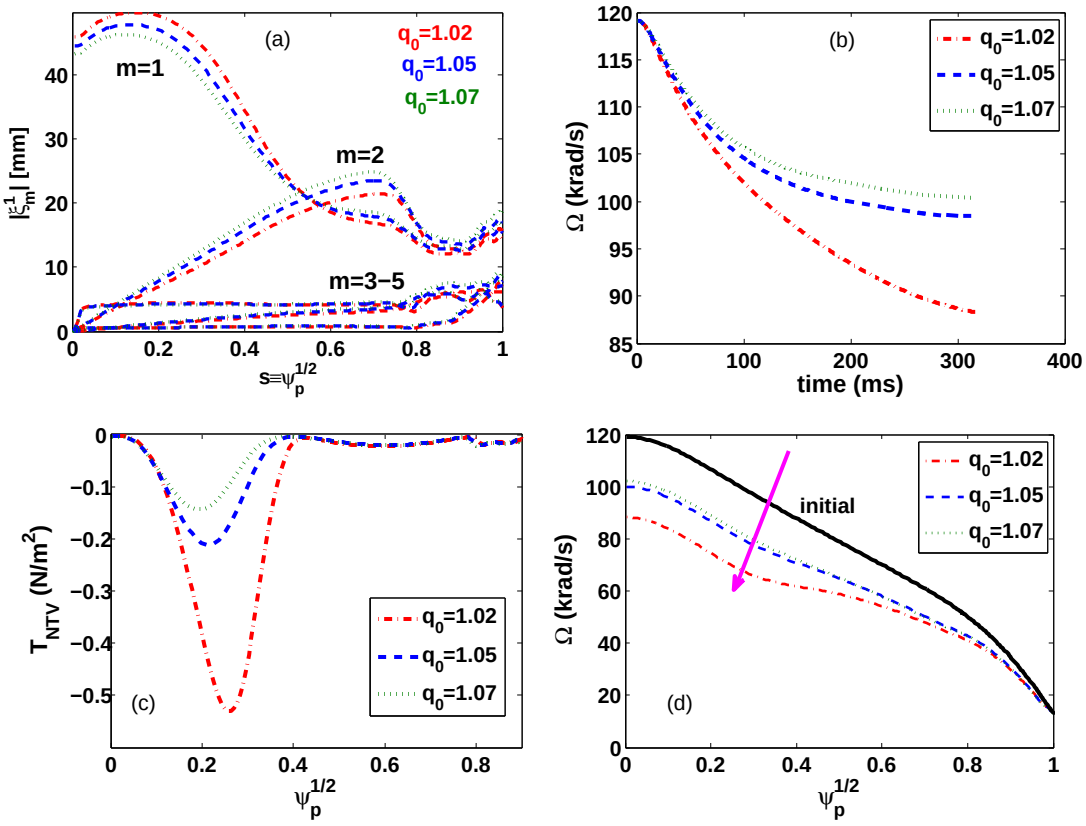

Figure 13: Comparison of various computed quantities for the different on-axis safety factors ($q_0 = 1.02, 1.05, 1.07$): (a) the poloidal Fourier harmonics of the computed plasma radial displacement (only the harmonics with $m = 1 \sim 5$ are presented). The time evolution of (b) the amplitude of the plasma rotation at the magnetic axis, and (c) the radial profile of the final NTV torque, and (d) the radial profile of the final plasma rotation. The RMP coil current is assured to be even parity ($\Delta\phi^{U/L} = 0$).

density profile. Thus the shape of the q-profile is largely unchanged. Figure 13(a) compares amplitude of the poloidal Fourier harmonics ($m = 1 \sim 5$) of the radial displacement, computed with linear response and assuming three q_0 values: 1.02, 1.05 and 1.07, respectively. As expected, the internal kink response becomes weaker with increasing q_0. But the effect is not dramatic.

Results from quasi-linear simulations are compared in plots Fig. 13(b-d), for the aforementioned three equilibria. Increasing the q_0 value (away from 1) leads to less core flow damping (Fig. 13(b,d)). This is largely due to less NTV torque produced in the

plasma core region at elevated q-profile (Fig. 13(c)). On the other hand, we find that the core plasma flow damping is generally less sensitive to q_0, as compared to varying other parameters (plasma equilibrium pressure, initial flow amplitude, RMP coil phasing).

6. Summary and conclusion

Both linear and quasi-linear plasma response to the $n = 1$ resonant magnetic perturbation (RMP) field is modelled, for a high-beta hybrid ASDEX Upgrade discharge. The linear response computations reveal that a large internal kink component is triggered by the RMP. As a result, large quasi-linear neoclassical toroidal viscous (NTV) torque is produced in the plasma core region, which dominates over other toroidal torques (the Maxwell and Reynolds stress torques). The NTV torque is significantly enhanced by mode-particle resonances at slow plasma flow, by entering into the so-called super-banana regime.

For the reference ASDEX Upgrade plasma, MARS-Q quasi-linear initial value modelling shows 25% of the plasma core flow damping (largely by the NTV torque). This result agrees well with the experimental observation.

Furthermore, systematic scans of various parameters lead to the following conclusions.

(i) The finite flow damping in this ASDEX Upgrade discharge is a result of large plasma amplification to the applied RMP field at high beta, yielding a large core NTV torque. Lowering the plasma beta, by a factor of ~ 2, results in almost no core flow damping. The measurement of the plasma beta value should be reasonably accurate (well within a factor of 2) in experiments. Therefore, we do not expect that the MARS-Q simulation results change much within the experimental uncertainty in plasma pressure.

(ii) Larger flow damping is obtained if the plasma initial flow is reduced. This is associated with both the better resonance condition at slow flow, and the larger internal kink response at slow flow. Full damping of flow is also obtained in MARS-Q modelling with reduced initial flow. The assumed two initial flow profiles in this study have larger variation than the experimental uncertainty in the toroidal rotation measurement, yet the fraction of the flow reduction is similar ($\sim$25% at faster rotation versus $\sim$30% at slower rotation) in these two simulations, if we ignore the second flow damping phase due to mode locking in the case of slower initial flow. Including this second phase damping, the MARS-R simulation with slower initial flow produces result that is more close to the experimental observation.

(iii) By scanning the relative toroidal phase of the B-coil currents between upper and lower rows, we find that the maximal (minimal) linear plasma response occurs when the $\Delta\phi^{U/L}$ is about 20 (200) degrees. Quasi-linear simulations show appreciable flow damping by the maximal response ($\Delta\phi^{U/L} = 20^o$), whilst almost no flow damping by the minimal response ($\Delta\phi^{U/L} = 200^o$). These results are quantitatively consistent with the experimental observations in ASDEX Upgrade.

(iv) The internal kink response decreases with increasing equilibrium core safety

factor further above 1. This produces a weaker plasma flow damping, but the effect is less dramatic as compared to that caused by the aforementioned parameters. On the other hand, the experimental uncertainty in the on-axis safety factor value may not be small. In terms of quantitative comparison with the measured flow damping, our simulation results favor the assumption of q_0 being very close to 1 (i.e. q_0 below 1.02).

Overall, this work points to the important role played by the internal kink response in plasma core flow damping in high-beta hybrid scenario plasmas. Similar quantitative study need to be carried out for ITER hybrid scenarios. The role of the NTV toque may be even more pronounced in ITER plasmas, because of both lower collisionality and slower toroidal flow expected for ITER.

Acknowledgments

This work is supported by National Natural Science Foundation of China under Contact No. 11805054, 11775069, 11675050, 11605046, National Key R&D Program of China under Contact No. 2017YFE0301201, National Magnetic Confinement Fusion Science Program of China under Contact No. 2015GB104004. The work is also supported by US DoE Office of Science under Contract DE-FG02-95ER54309 and DE-FC02-04ER54698. This work is also partly supported by the EUROfusion Consortium. The views and opinions expressed herein do not necessarily reflect those of the European Commission.

References

[1] Sips A.C.C. *et al* 2002 *Plasma Phys. Control. Fusion* **44** B69
[2] Luce T.C. *et al* 2014 *Nucl. Fusion* **54** 013015
[3] Petty C.C. *et al* 2015 *Nucl. Fusion* **55** 016016
[4] Evans T.E. *et al* 2004 *Phys. Rev. Lett.* **92** 235003
[5] Liang Y. *et al* 2007 *Phys. Rev. Lett.* **98** 265004
[6] Suttrop W. *et al* 2011 *Phys. Rev. Lett.* **106** 225004
[7] Kirk A. *et al* 2011 *Plasma Phys. Control. Fusion* **53** 065011
[8] Jeon Y.M. *et al* 2012 *Phys. Rev. Lett.* **109** 035004
[9] Sun Y. *et al* 2016 *Phys. Rev. Lett.* **117** 115001
[10] Reimerdes H. *et al* 2005 *Nucl. Fusion* **45** 368
[11] Liu Y.Q. *et al* 2010 *Plasma Phys. Control. Fusion* **52** 045011
[12] Lanctot M.J. *et al* 2010 *Phys. Plasmas* **17** 030701
[13] Gryaznevich M.P. *et al* 2008 *Plasma Phys. Control. Fusion* **50** 124030
[14] Piovesan P. *et al* 2017 *Plasma Phys. Control. Fusion* **59** 014027
[15] Zhu W. *et al* 2006 *Phys. Rev. Lett.* **96** 225002
[16] Hua M.D. *et al* 2010 *Plasma Phys. Control. Fusion* **52** 035009
[17] Sun Y. *et al* 2010 *Plasma Phys. Control. Fusion* **52** 105007
[18] Frassinetti L. *et al* 2015 *Nucl. Fusion* **55** 112003
[19] Logan N.C. *et al* 2016 *Nucl. Fusion* **56** 036008
[20] Kim K. *et al* 2017 *Nucl. Fusion* **57** 126035
[21] Li X.Y. *et al* 2019 *Phys. Plasmas* **26** 052512
[22] Liu Y.Q. *et al* 2012 *Phys. Plasmas* **19** 102507
[23] Liu Y.Q. *et al* 2015 *Nucl. Fusion* **55** 063027
[24] Liu Y.Q. *et al* 2000 *Phys. Plasmas* **7** 3681

[25] Liu Y.Q. *et al* 2013 *Phys. Plasmas* **20** 042503
[26] Liu Y.Q. *et al* 2010 *Phys. Plasmas* **17** 122502
[27] Haskey S. *et al* 2014 *Nucl. Fusion* **56** 035005
[28] Chapman I.T. *et al* 207 *Nucl. Fusion* **47** L36
[29] Shaing K.C. *et al* 2015 *Nucl. Fusion* **55** 125001
[30] Liu Y.Q. *et al* 2016 *Plasma Phys. Control. Fusion* **58** 114005
[31] Zhang N. *et al* 2018 *Phys. Plasmas* **25** 092502
[32] Hammett G.W. *et al* 1990 *Phys. Rev. Lett.* **64** 3019
[33] Shaing K.C. *et al* 2010 *Nucl. Fusion* **50** 025022
[34] Sun Y. *et al* 2011 *Nucl. Fusion* **51** 053015
[35] Zhang N. *et al* 2017 *Phys. Plasmas* **24** 082507
[36] Liu Y.Q. *et al* 2012 *Plasma Phys. Control. Fusion* **54** 124013
[37] Mc Carthy P.J. *et al* 2012 *Plasma Phys. Control. Fusion* **54** 015010
[38] Lütjens H. *et al* 1996 *Comput. Phys. Commun.* **97** 219
[39] Suttrop W. *et al* 2009 *Fusion Eng. Des.* **84** 290